Determination of Parton Densities for QCD partons and Electroweak Bosons

K. Moral Figueroa¹, E. Gallo¹, H. Jung^{1,2,3}, and S. Taheri Monfared¹

¹Deutsches Elektronen-Synchrotron DESY, Germany ²Elementary Particle Physics, University of Antwerp, Belgium ³II. Institut für Theoretische Physik, Universität Hamburg, Germany

Abstract

Parton densities are obtained from a solution of the extended DGLAP-type evolution equation that includes both QCD and electroweak contributions. The equations are solved using the Parton-Branching (PB) approach, and the evolution is performed at next-to-leading order for QCD partons and leading order for electroweak bosons.

The initial QCD parton distributions are fitted to HERA deep inelastic scattering data, while photon and weak-boson densities are generated perturbatively and validated against $d\sigma/dQ^2$.

The resulting collinear and transverse-momentum dependent (TMD) densities are provided in LHApdf and TMDlib formats for direct phenomenological use.

1 Introduction

Predictions for high-energy hadronic processes rely on the factorization of perturbative and non-perturbative components. The parton densities themselves consist of a perturbative part (the perturbative evolution equations) and the non-perturbative input distributions at a scale of the order of the hadron mass. Several collaborations, such as CTEQ [1–3], MSHT [4–7] and NNPDF [8, 9] have performed precise global fits of QCD parton densities. A public tool, xFitter [10, 11], exists for the fitting framework. QCD parton and photon densities are now determined by all groups, but heavy boson densities are not yet available in parameterized form (in the parton-density repository LHAPDF [12]). In this publication we describe the determination of a complete set of parton densities* for QCD partons as well as for the electroweak bosons: γ , Z and W.

The factorization framework simplifies complex hadronic processes and offers physical insight through the picture of parton branching. The Effective W/Z Approximation (EWA) [13–16] involves the partitioning of collinear, initial-state W/Z boson emissions out of matrix elements (MEs) into collinear parton density functions (PDFs). This approximation, as an extension of the Equivalent Photon Approximation (EPA) [17, 18] (or Weizsäcker-Williams Approximation [19,20]), offers significant computational benefits, particularly dealing with infrared limits of phase space and avoiding numerical instabilities in calculations when scale hierarchies are present. A concise derivation of the equivalent vector-boson approximation is given in Ref. [21]. The concept of EWA has already been used in calculations including weak vector boson fusion (VBF) [22–26] and heavy quark production via Wg-scattering [22, 27]. Renewed interest in the EWA came with the discussion of high energy muon colliders [28].

Recently, collinear parton densities including electroweak (EW) bosons have been discussed in more complete approaches [29–32]. Electroweak evolution equations are discussed in [33–35]. Splitting functions for W-emission including a transverse momentum dependence have been calculated in Ref. [36]. On the experimental side, measurements of jets and EW bosons at the LHC [37,38] support the picture, that at high energies the radiation of massive EW bosons from light quarks [39] can be treated similarly to those of massless photons or gluons.

In this study, we present a solution of the extended DGLAP evolution equation including the photon and heavy electroweak bosons. We apply the Parton Branching (PB) method [40, 41] for solving the evolution equation. This method (as already implemented in the evolution package UPDFEVOLV2 [42]) has the advantage that implementing additional boson contributions and kinematic constraints is straightforward. Together with the determination of collinear parton densities, Transverse Momentum Dependent (TMD) densities are also calculated.

We discuss in Chapter 2 the evolution equations and introduce the splitting functions and couplings for EW bosons. We also discuss the treatment of heavy boson masses. In Chapter 3 we describe the fit of the initial conditions of the strongly interacting partons to precision measurements obtained at HERA and the determination of parton distributions. We also

^{*}We use the wording parton density for partons but also for electroweak bosons.

show a validation of the heavy boson densities, using measurements of $d\sigma/dQ^2$ obtained at HERA for both neutral and charged currents. Conclusions are given in Chapter 4.

2 Evolution equations for QCD partons and electroweak bosons

The evolution of parton densities with scale μ^2 is described by the DGLAP equation [43–46]:

$$\mu^2 \frac{\partial x f_a(x, \mu^2)}{\partial \mu^2} = \sum_b \int_x^1 dz \ P_{ab} \left(\alpha_{\text{eff}}(\mu^2), z \right) \ \frac{x}{z} f_b \left(\frac{x}{z}, \mu^2 \right) \ , \tag{1}$$

where P_{ab} denotes the regularized splitting function for the transition $b \to a$, which can be decomposed as (in the notation of Ref. [40]):

$$P_{ab}(z, \alpha_{\text{eff}}) = D_{ab}(\alpha_{\text{eff}})\delta(1-z) + K_{ab}(\alpha_{\text{eff}})\frac{1}{(1-z)_{+}} + R_{ab}(z, \alpha_{\text{eff}}).$$
 (2)

The splitting functions for QCD partons are known, and summarized for NLO and NNLO in Ref [47–57]. Photon and heavy-boson radiation from quarks occurs analogously to gluon emission. In the PB approach, the evolution equations are rewritten using Sudakov form factors, which replace the plus-prescription and allow a probabilistic interpretation, as discussed in detail in Refs. [40,41]. The coupling $\alpha_{\rm eff}$ is the effective coupling, dependent on the parton (particles) involved, for QCD partons $\alpha_{\rm eff} = \alpha_{\rm s}$.

The evolution equation in terms of Sudakov form factors $\Delta_a^S(\mu^2)$ is given by:

$$xf_a(x,\mu^2) = \Delta_a^S(\mu^2) xf_a(x,\mu_0^2) + \sum_b \int_{\mu_0^2}^{\mu^2} \frac{dq^2}{q^2} \frac{\Delta_a^S(\mu^2)}{\Delta_a^S(q^2)} \int_x^{z_{\rm M}} dz \frac{\alpha_{\rm eff}}{2\pi} \hat{P}_{ab}(z) \frac{x}{z} f_b\left(\frac{x}{z},q^2\right) . \tag{3}$$

The limiting scale $z_{\rm M}$ in the z-integral is important in this prescription, since to be consistent with the DGLAP equations for massless QCD partons and the photon, the integration limit $z_{\rm M} \to 1$ (for the numerical calculations we use $z_{\rm M} = 1 - \epsilon$, with ϵ being small). The Sudakov form factor is given by:

$$\Delta_a^S(\mu^2) = \Delta_a^S(z_{\rm M}, \mu^2, \mu_0^2) = \exp\left(-\sum_b \int_{\mu_0^2}^{\mu^2} \frac{dq^2}{q^2} \int_0^{z_{\rm M}} dz \, z \frac{\alpha_{\rm eff}}{2\pi} \, P_{ba}^{(R)}(z)\right) , \qquad (4)$$

In the PB-approach, the evolution equation for collinear densities is extended to include also transverse momenta of the partons (and bosons). After identifying the evolution scale with a physical scale, here the rescaled transverse momentum (coming from angular ordering), transverse momenta of the emitted partons can be calculated, as described in detail in Ref. [40,41].

The calculation of collinear photon densities has been discussed quite extensively in literature, see e.g. Refs. [5,58–65]. For a complete description of the photon density, also an intrinsic distribution of photons inside the hadron must be included, which is relevant at

small scales μ^2 , while at large scales the dominant contribution comes from photon radiation off the quarks. Several groups [5, 60, 63] allow and treat an intrinsic photon component inside the proton. In the approach described here, we neglect any initial photon contribution, since we are interested in the contribution at large scales and aim for a consistent treatment of photon and heavy boson densities. The determination of effective W densities has already been discussed in Refs. [13–16,25,66–69] and in recent years, these ideas have been revisited in Refs. [29–31,35,70].

The effective coupling α_{eff} (given in Tab. B) for photons is $\alpha_{\text{eff}} = \alpha_{\text{em}}$, while for processes with Z or W it can be obtained from the total production $q_i\bar{q}_j$ -cross section, and is given by:

$$Z: \alpha_{\text{eff}} = \frac{\alpha_{\text{em}}}{4\sin^2\theta_{\text{W}}\cos^2\theta_{\text{W}}} (V_f^2 + A_f^2)$$
 (5)

$$W: \alpha_{\text{eff}} = \frac{\alpha_{\text{em}} |V_{qq}|^2}{4\sin^2 \theta_W}, \qquad (6)$$

with θ_W being the Weinberg angle and V_f , A_f being the vector and axial couplings of the Z-boson to the fermions, and V_{qq} being the CKM element.

In the massless limit, the splitting functions for EW processes at LO are identical to the corresponding ones of QCD partons modulo the coupling and different color factors (as given in Tab. B), and the self-coupling, which does not exist for photons (the treatment of heavy boson masses is discussed in Section 2.1). In Appendix B we give an overview of the EW splitting functions at leading order. We average over all transverse polarization states, and neglect any longitudinal contribution from γ -, Z- and W- contribution (only in section 3.5 for the validation with the DIS cross section, we need to obtain W- densities with different polarization states). A full account including different polarization states is given in Refs. [29,31,32,35,70].

We show here explicitly the momentum weighted density for photons, Z- and W-bosons:

$$\mu^{2} \frac{\partial x f_{\gamma}(x,\mu^{2})}{\partial \mu^{2}} = \int_{x}^{1} dz \, P_{\gamma q} \left(\alpha_{\text{eff}}(\mu^{2}), z \right) \, \sum_{i} e_{i}^{2} \left[\frac{x}{z} f_{i} \left(\frac{x}{z}, \mu^{2} \right) + \frac{x}{z} \bar{f}_{i} \left(\frac{x}{z}, \mu^{2} \right) \right]$$

$$= \frac{\alpha_{\text{em}}}{2\pi} \int_{x}^{1} \frac{dz}{z} \left(1 + (1 - z)^{2} \right) \sum_{u,d} e_{i}^{2} \left[\frac{x}{z} F_{i} \left(\frac{x}{z}, \mu^{2} \right) + \frac{x}{z} \bar{F}_{i} \left(\frac{x}{z}, \mu^{2} \right) \right]$$

$$\mu^{2} \frac{\partial x f_{Z}(x,\mu^{2})}{\partial \mu^{2}} = \frac{\alpha_{\text{em}}}{8\pi \sin^{2} \theta_{W} \cos^{2} \theta_{W}} \int_{x}^{1} \frac{dz}{z} \left(1 + (1 - z)^{2} \right)$$

$$\times \sum_{u,d} \left(V_{i}^{2} + A_{i}^{2} \right) \left[\frac{x}{z} F_{i} \left(\frac{x}{z}, \mu^{2} \right) + \frac{x}{z} \bar{F}_{i} \left(\frac{x}{z}, \mu^{2} \right) \right]$$

$$\mu^{2} \frac{\partial x f_{W^{-}}(x,\mu^{2})}{\partial \mu^{2}} = \frac{\alpha_{\text{em}}}{8\pi \sin^{2} \theta_{W}} |V_{qq}|^{2} \int_{x}^{1} \frac{dz}{z} \left(1 + (1 - z)^{2} \right) \frac{x}{z} \left[D \left(\frac{x}{z}, \mu^{2} \right) + \bar{D} \left(\frac{x}{z}, \mu^{2} \right) \right]$$

$$\mu^{2} \frac{\partial x f_{W^{+}}(x,\mu^{2})}{\partial \mu^{2}} = \frac{\alpha_{\text{em}}}{8\pi \sin^{2} \theta_{W}} |V_{qq}|^{2} \int_{x}^{1} \frac{dz}{z} \left(1 + (1 - z)^{2} \right) \frac{x}{z} \left[U \left(\frac{x}{z}, \mu^{2} \right) + \bar{D} \left(\frac{x}{z}, \mu^{2} \right) \right]$$

$$\mu^{2} \frac{\partial x f_{W^{+}}(x,\mu^{2})}{\partial \mu^{2}} = \frac{\alpha_{\text{em}}}{8\pi \sin^{2} \theta_{W}} |V_{qq}|^{2} \int_{x}^{1} \frac{dz}{z} \left(1 + (1 - z)^{2} \right) \frac{x}{z} \left[U \left(\frac{x}{z}, \mu^{2} \right) + \bar{D} \left(\frac{x}{z}, \mu^{2} \right) \right]$$

$$\mu^{2} \frac{\partial x f_{W^{+}}(x,\mu^{2})}{\partial \mu^{2}} = \frac{\alpha_{\text{em}}}{8\pi \sin^{2} \theta_{W}} |V_{qq}|^{2} \int_{x}^{1} \frac{dz}{z} \left(1 + (1 - z)^{2} \right) \frac{x}{z} \left[U \left(\frac{x}{z}, \mu^{2} \right) + \bar{D} \left(\frac{x}{z}, \mu^{2} \right) \right]$$

$$\mu^{2} \frac{\partial x f_{W^{+}}(x,\mu^{2})}{\partial \mu^{2}} = \frac{\alpha_{\text{em}}}{8\pi \sin^{2} \theta_{W}} |V_{qq}|^{2} \int_{x}^{1} \frac{dz}{z} \left(1 + (1 - z)^{2} \right) \frac{x}{z} \left[U \left(\frac{x}{z}, \mu^{2} \right) + \bar{D} \left(\frac{x}{z}, \mu^{2} \right) \right]$$

where we have introduced the following combinations of the quark densities $f_i(x, Q^2)$:

$$xF_u = xU = xu + xc, x\bar{F}_u = x\bar{U} = x\bar{u} + x\bar{c}, \tag{11}$$

$$xF_d = xD = xd + xs, x\bar{F}_d = x\bar{D} = x\bar{d} + x\bar{s}$$

$$\tag{12}$$

2.1 Mass treatment for Heavy Bosons

In the Zero-Mass-Variable-Flavor-Number-Scheme (ZMVFN) used for QCD partons, all partons are treated massless. Heavy-flavors are only produced, once the scale is above the heavy flavour mass. An analogous scheme is applied for heavy bosons. However, measurements of charged-current cross sections in lepton-proton collisions give a non-zero cross section for $Q^2 < M_W^2$, suggesting the application of a suppression factor $\left[\frac{Q^2}{Q^2+M_W^2}\right]^2$. In an approach applying angular ordering, the mass of the emitted (or emitting) parton can limit the range in z-integration by $z_{\rm M}=1-\frac{M}{a}$.

We now summarize three mass-treatment scenarios (referred to as MASSCUTSCHEME):

• MASSCUTSCHEME=0: In the ZMVFN scheme, the heavy boson mass M_V is included as a mass threshold as applied in the EWA [28]:

$$\alpha_{\text{eff}} \equiv \alpha_{\text{eff}} \cdot \Theta \left(q^2 - M_V^2 \right) \tag{13}$$

• MASSCUTSCHEME=1: The boson mass M_V is treated by a suppression factor [29] (similar to the treatment in the DIS cross section):

$$\alpha_{\text{eff}} \equiv \alpha_{\text{eff}} \cdot \left[\frac{q^2}{q^2 + M_V^2} \right]^2 \,.$$
 (14)

This is taken as the default scenario.

• MASSCUTSCHEME=2: In angular ordering, the boson mass M_V is included via a limit in the z integrals [31] (and thus also in α_{eff}):

$$\alpha_{\text{eff}} \equiv \alpha_{\text{eff}} \cdot \Theta \left(q^2 (1 - z)^2 - M_V^2 \right) \text{ and } z_{\text{M}} = 1 - \frac{M_V}{q}$$
 (15)

In the first two cases, $z_{\rm M} \to 1$, while in MASSCUTSCHEME=2 the z-integration is limited. In all cases, the splitting functions are taken in the massless limit. The different choices will lead to different collinear and in particular, transverse momentum dependent distributions.

3 QCD fits of initial parton distributions

We determine the initial collinear and TMD distributions using the PB-method, fitting to precision DIS cross-section data from HERA [71], as detailed in Ref. [72]. The application of

the extended evolution equation eq. (1), including photons and electroweak bosons requires a new determination of the initial parameters, because additional radiation of photons and electroweak bosons off quarks will lead to a reduction of the quark densities. The determination of the parton densities is performed under the following assumptions: a.) the initial photon density is ignored in order to keep the same structure as for heavy boson densities, b.) interference of γ and Z is ignored during the evolution, and c.) the DIS structure functions are unchanged compared to the NLO QCD case, since the electroweak contributions are considered only at LO (see discussion in Ref. [73]).

We perform new fits of the initial parameters to obtain a complete set of QCD and EW parton densities. We follow the same strategy as in Ref. [72] and determine two different sets of distributions, labeled as Set1[†] and Set2: in Set 1, we use $\alpha_s(q)$ while in Set 2 $\alpha_s(q_t)$ is applied with q being the virtuality of the propagating parton, and q_t is the transverse momentum of the emitted parton with $q_t = q(1-z)$.

Studies of the transverse momentum distribution of DY lepton pairs at the LHC showed, that the limit of $z_{\rm M}=1-q_0/q$ with $q_0=0.01$ GeV as used in PB-NLO-2018 Set2 was leading to a small energy dependence of the determined intrinsic $k_{\rm T}$ -distribution, while using a much smaller $q_0=0.00001$ GeV gave an \sqrt{s} independent intrinsic $k_{\rm T}$ -distribution [75]. For the new densities, which we label PB-NLO-QCD+EW-2025, we take this observation into account by consistently using $z_{\rm M}$ as a technical parameter with $z_{\rm M} \to 1$ using $z_{\rm M}=0.99999$.

The QCD part of the evolution is treated at next-to-leading order (NLO) in both $\alpha_{\rm s}$ and the splitting functions, while the electroweak part (photon and electroweak boson) is taken with leading order splitting functions. This so-called "phenomenological" approach [59] is taken, since $\alpha_{\rm s}^2 \sim \alpha_{\rm em}$, in contrast to a "democratic" approach, where the same order in the perturbative expansion is used. In the calculations we take $\alpha_{\rm em}=1/137$ fixed since different scale choices for electroweak processes are less clear and require a further detailed study. The scheme of electroweak parameters used is given in Appendix A. The heavy boson mass is treated with MASSCUTSCHEME=1. The other two schemes, discussed in the previous section, are used for comparison only.

We use the xFitter package [10] and use several advantages in the new package (multi-thread, Ceres minimizer better suited for Monte Carlo generated grid files) compared to the fit reported in Ref. [72]. We apply the same form of parameterization for the QCD starting distributions, same starting scale and heavy flavor masses. Including photon and heavy-boson evolution slightly increases χ^2 compared to the pure-QCD fit (Tab. 1).

3.1 Uncertainties

Uncertainties of the distributions are obtained, as described in Ref. [72]: uncertainties coming from the statistical and systematic uncertainties of the measurements are estimated using the Pumplin method [76] (as implemented in xFitter), and model uncertainties are obtained by

[†]Although, for the transverse momentum distributions of Drell-Yan (DY) lepton pair, Set2 (with $\alpha_s(q_t)$) describes the measurements much better (see Refs. [74,75]), for most of the calculations using collinear parton distributions the strategy of Set1 (using $\alpha_s(q)$) is used.

PB NLO Set 1 $lpha_{ m s}(q^2)$						
	χ^2	d.o.f	$\chi^2/\text{d.o.f}$			
PB-NLO-QCD-2025 Set1	1361	1131	1.20			
PB-NLO-QCD+EW-2025 Set1	1378	1131	1.22			
PB NLO Set 2 $lpha_{ m s}(q_{ m t}^2)$						
	χ^2	d.o.f	$\chi^2/\text{d.o.f}$			
PB-NLO-QCD-2025 Set2	1388	1131	1.23			
PB-NLO-QCD+EW-2025 Set2	1396	1131	1.24			

Table 1: Values of χ^2 for the different Sets at NLO.

new fits with changed heavy quark masses, starting values μ_0^2 for the evolution and q_{min} for Set2, as described in Tab. 2.

The most dominant part of the uncertainties of the electroweak densities comes from the uncertainties of the quark distributions at large x, both from the statistical and systematic uncertainties coming from the measurements as well as from model uncertainties of the QCD partons. Additional uncertainties of the electroweak contributions come from uncertainties in the coupling, as well as the masses of the heavy bosons (for the uncertainties given by PDG [77] see Appendix A). These uncertainties are much smaller than those coming from the uncertainties of the determination of the QCD parton distributions. We have varied $m_{\rm Z}$ and $m_{\rm W}$ by ± 0.1 GeV and calculated the distributions and found effects much smaller than the other model uncertainties, and thus neglected those variations.

	Central	Lower	Upper
	value	value	value
PB-NLO-QCD+EW-2025 Set 1 μ_0^2 (GeV ²)	1.9	1.6	2.2
PB-NLO-QCD+EW-2025 Set 2 μ_0^2 (GeV ²)	1.4	1.1	1.7
PB-NLO-QCD+EW-2025 Set 2 q_{min} (GeV)	1.0	0.9	1.1
m_c (GeV)	1.47	1.41	1.53
m_b (GeV)	4.5	4.25	4.75

Table 2: Central values and change ranges of parameters for model dependence

3.2 QCD parton densities

In Fig. 1 we compare collinear quark and gluon densities at $\mu=100$ GeV obtained from the full set (including QCD and EW effects, PB-NLO-QCD+EW-2025) to the one with QCD partons only (PB-NLO-QCD-2025). The distributions, including electroweak bosons, are slightly different compared to those containing only QCD partons. The uncertainties shown in Fig. 2 do not fully cover these differences.

In Fig. 2 we compare distributions obtained from PB-NLO-QCD+EW-2025 Set1 and Set2. Uncertainties, obtained as described in Sec. 3.1, are shown in the lower panels. At small x

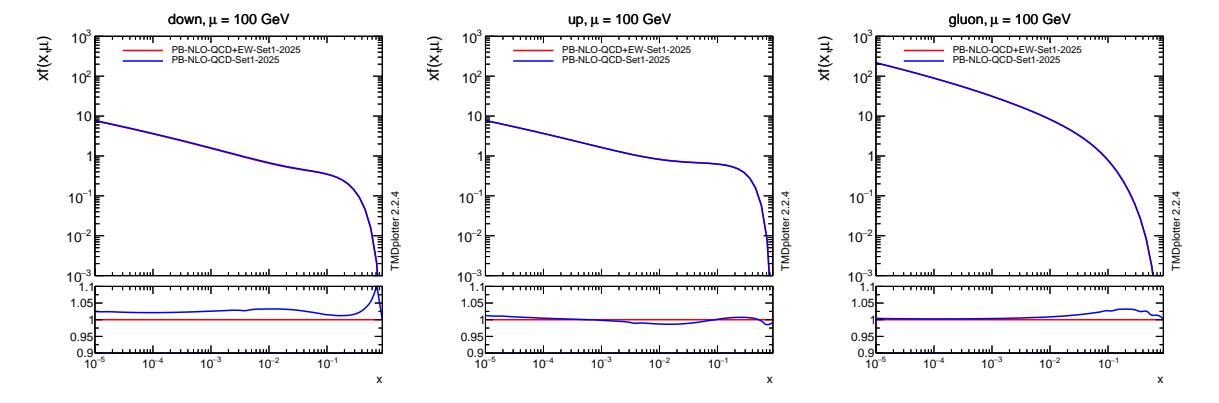


Figure 1: The collinear quark and gluon densities for Set1 at $\mu = 100$ GeV as a function of x. The EW set together with the one containing only QCD partons is shown. The lower panel shows the ratio between both.

there are small differences in the quark distributions, the gluon distribution differs at large x. These differences come from the different treatment of the scale used in $\alpha_{\rm s}$: in Set 1 the evolution scale q is used, while in Set2 the transverse momentum $q_{\rm t}$ is applied. In Fig. 10 in Appendix C we show the TMD distributions for quarks and gluons at $\mu=100$ GeV and x=0.01.

3.3 Photon densities

The collinear photon density, obtained from the fit[‡], as a function of x for different values of the evolution scales μ is shown in Fig. 3 for PB-NLO-QCD+EW-2025 Set1 and PB-NLO-QCD+EW-2025 Set2. The uncertainties shown come from the experimental and model uncertainties, as described in Sec. 3.1. For comparison the MSHT20qed photon densities [6] are shown. The inelastic component, comparable with the photon density described in this paper is shown separately. Rather good agreement is observed, the small differences come from α_{em} , which is taken as $\alpha_{em} = \alpha_0 = 1/137$ for consistency with the electroweak parameters.

In Fig. 11 of Appendix C the TMD density of photons is shown.

3.4 Heavy Boson densities

The approach to determine the photon densities within the PB-method has been extended to determine the collinear and TMD densities of Z and W as described in eqs.(8-10). The collinear densities for Z and W are shown in Figs. 4 and 5 using MASSCUTSCHEME=1. The W⁺ and W⁻ densities are different, because of the different couplings to u- and d-quarks. The uncertainties shown come from the experimental uncertainties as well as model uncertainties as described in Sec. 3.1. The uncertainties coming from changing the heavy boson

[‡]There are small differences to the one published in Ref. [58] due to mistreatment of the number of flavors.

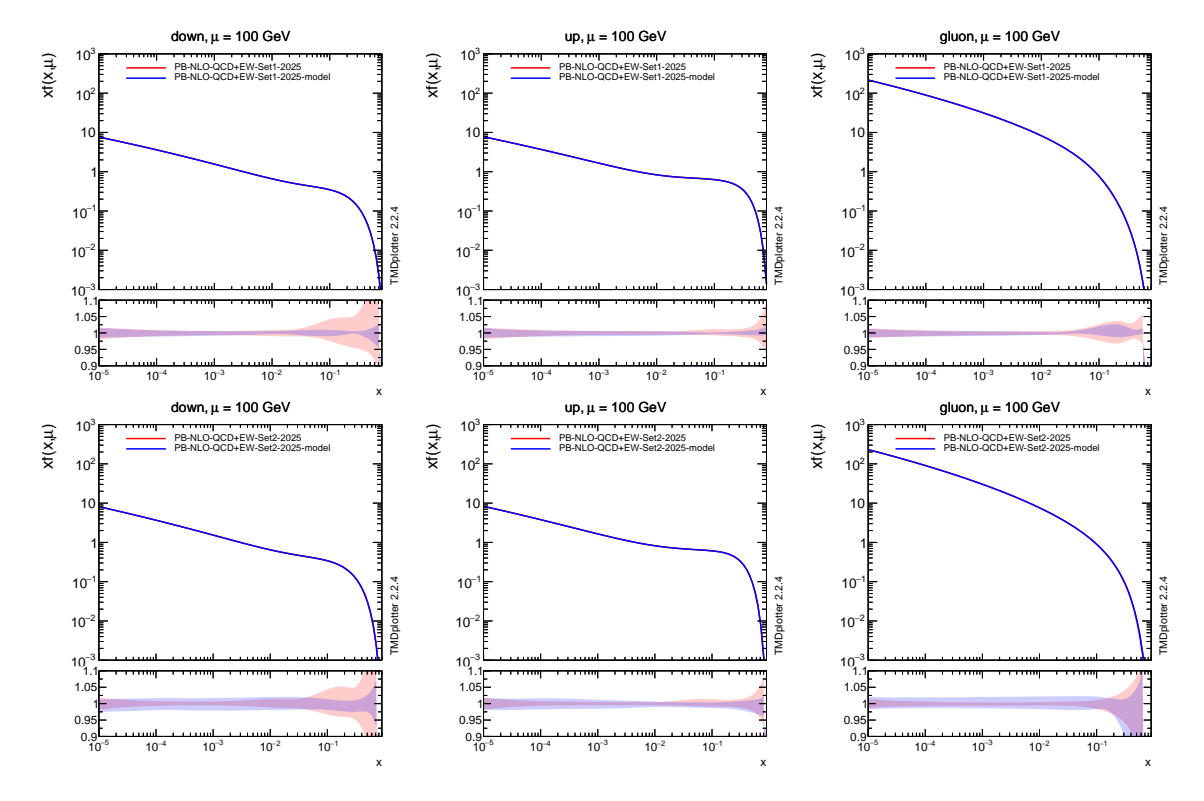


Figure 2: The collinear quark and gluon densities at $\mu = 100$ GeV as a function of x. Shown is PB-NLO-QCD+EW-2025 Set1 (upper row) and PB-NLO-QCD+EW-2025 Set2 (lower row). The uncertainty bands for experimental and model uncertainties are shown separately.

masses are much smaller than all the other uncertainties, and thus are neglected. The model uncertainties result from the large x-model dependence of the quark distributions, which can become significant.

The momentum fractions carried by photons, Z and W- bosons from $\int_0^1 dx x f(x,\mu)$ at $\mu=100~{\rm GeV^2}$ are shown in Tab. 3.

We now turn to the discussion of the different MassCutschemes: in Fig. 6 the collinear distribution for W-boson is shown as a function of x for different μ as obtained with the different MassCutschemes. The TMD distributions allow further insights into the behavior of the different MassCutschemes: in Fig. 7 the TMD distribution for the W-boson is shown for different μ as a function of k_T as obtained with the different MassCutschemes. Only MassCutscheme=1 gives a non-vanishing heavy boson density at low scales μ , while in the other schemes there is a mass cut and even MassCutscheme=2 (limiting the z-integral) results in a rather sharp threshold in k_T around the heavy boson mass (because

[§]In the TMD distributions fluctuations are visible which originate from the number of simulated events $(N=10^{10})$ in the forward evolution in UPDFEVOLV2.

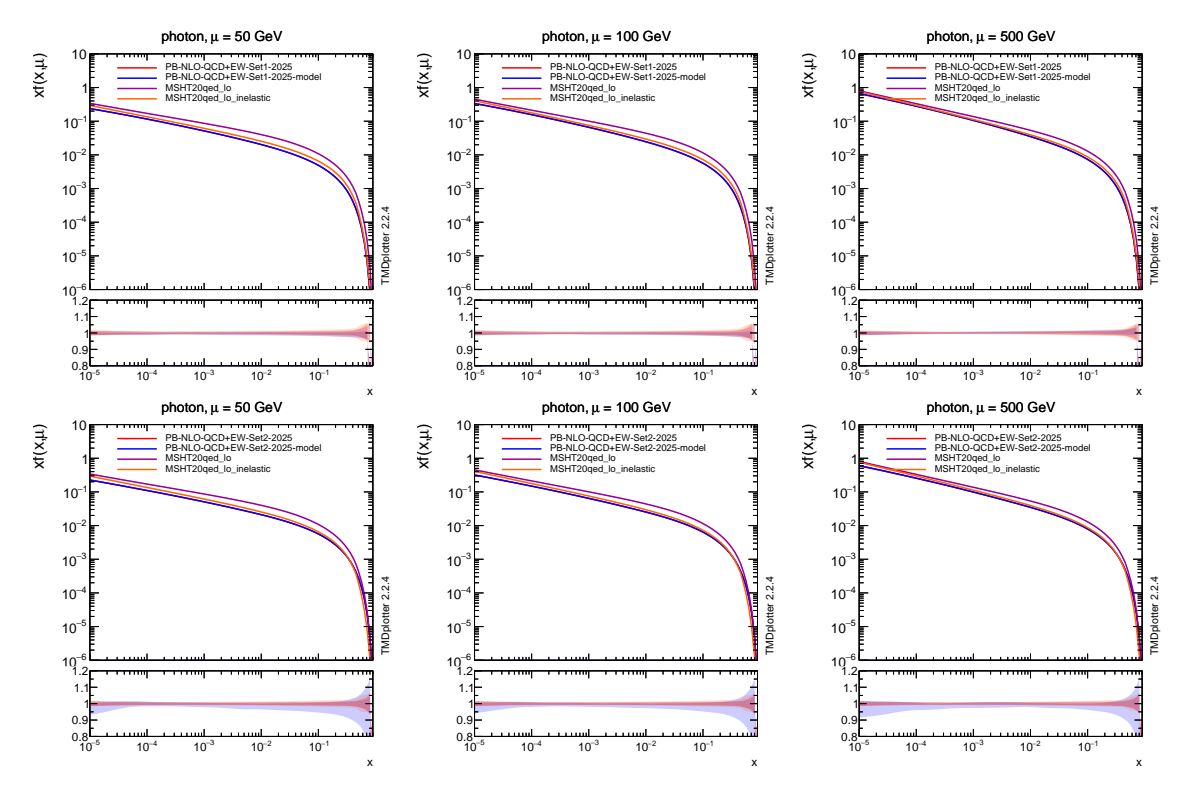


Figure 3: The collinear photon density for PB-NLO-QCD+EW-2025 Set1 (upper row) and Set2 (lower row) at $\mu=50$, 100 and 500 GeV as a function of x including experimental and model uncertainties. For comparison the prediction from MSHT20 [6] (total and inelastic) is shown.

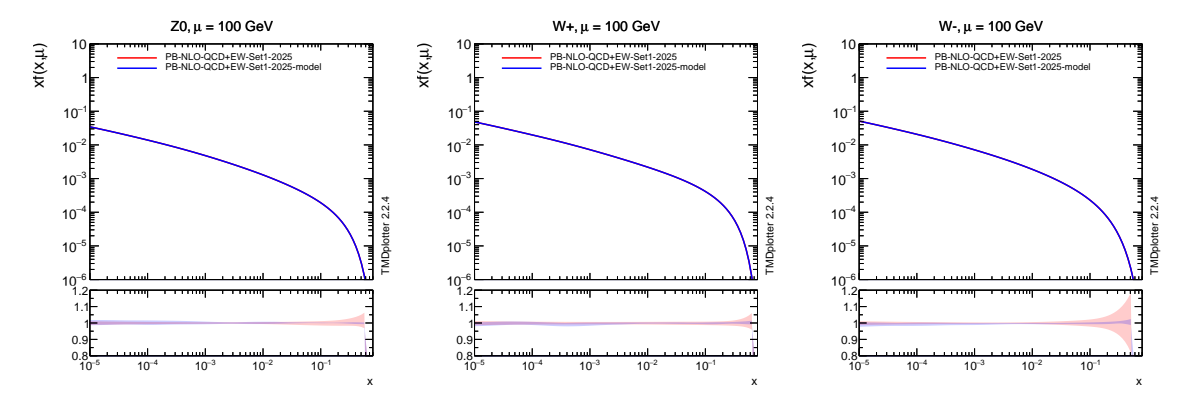


Figure 4: The collinear vector-boson densities for PB-NLO-QCD+EW-2025 Set1 at $\mu=100$ GeV as a function of x including experimental and model uncertainties.

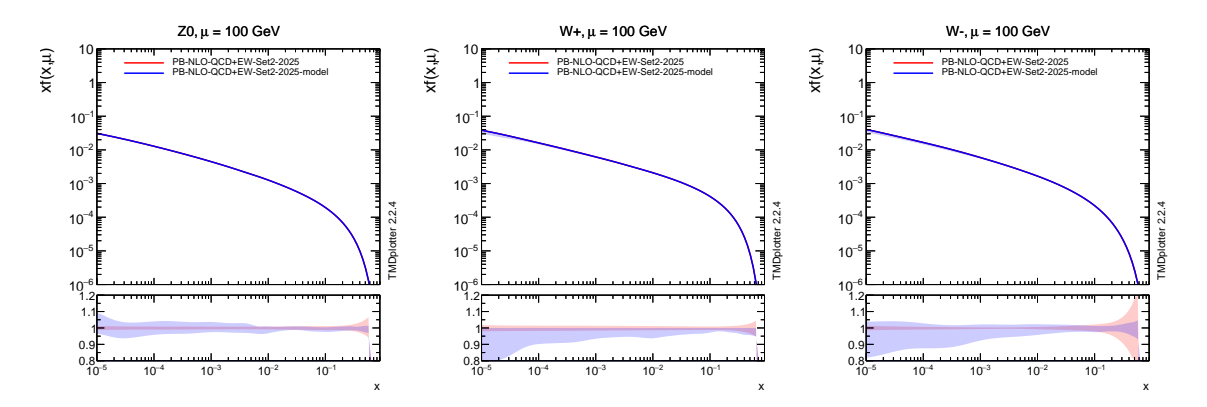


Figure 5: The collinear vector-boson density for PB-NLO-QCD+EW-2025 Set2 at $\mu = 100$ GeV as a function of x including experimental and model uncertainties.

$\int_0^1 dx x f_i(x,\mu)$	PB-NLO-QCD+EW-2025 Set1	PB-NLO-QCD+EW-2025 Set2	MSHT20qed_lo_inelastic
$i = \gamma$	0.0021	0.0023	0.0026
i = Z	$8.7 \cdot 10^{-5}$	$8.6 \cdot 10^{-5}$	-
$i = W^+$	$1.7 \cdot 10^{-4}$	$1.6 \cdot 10^{-4}$	_
$i = W^-$	$1.2 \cdot 10^{-4}$	$1.0 \cdot 10^{-4}$	-

Table 3: Momentum fraction $\int_0^1 dx \, x f(x,\mu)$ carried by γ , Z, and W for PB-NLO-QCD+EW-2025 Set1, PB-NLO-QCD+EW-2025 Set2 and MSHT20qed_lo_inelastic at $\mu=100$ GeV

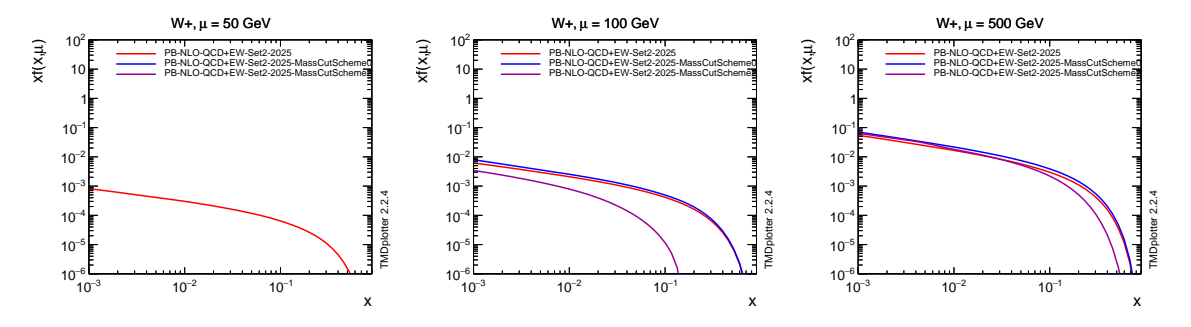


Figure 6: The collinear density for the W-boson for PB-NLO-QCD+EW-2025 Set2 at $\mu=50$, 100 and $\mu=500$ GeV as a function of x for the different MASSCUTSCHEMES.

of z=1-M/q). The contribution at small $k_{\rm T}$ obtained in MassCutscheme=2 comes from multiple emissions which are added vectorially, indicating that at a scale $\mu=500~{\rm GeV}$ the vector-boson is also undergoing evolution. We observe that at $\mu=500~{\rm GeV}$ the prediction from MassCutscheme=2 gives a larger density, compared to the one with MassCutscheme=1, because the suppression factor is still sizeable.

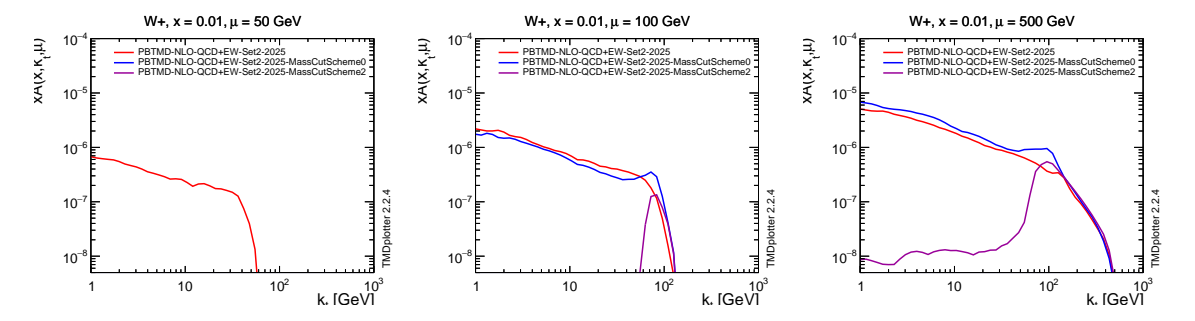


Figure 7: The TMD density for the W-boson for PB-NLO-QCD+EW-2025 Set2 at $\mu = 50$, 100 and $\mu = 500$ GeV as a function of $k_{\rm T}$ for the different MASSCUTSCHEMES.

For completeness, the TMD distributions for heavy bosons with the default MASS-CUTSCHEME=1 are shown in Fig. 12 of Appendix C.

In summary, the densities of heavy bosons depend over a large range of scales μ on the treatment of the heavy boson mass: a dynamical suppression factor as used in MASS-CUTSCHEME=1 offers a smooth description from small to high scales. The mass treatment MASSCUTSCHEME=2, motivated from angular ordering, leads to modifications of the TMD, but also the collinear densities for scales $\mu < m_{\rm Z}$. In order to obtain distributions applicable over a large range of μ , MASSCUTSCHEME=1 is used as the default.

3.5 Validation of electroweak boson densities with DIS cross sections

The DIS cross section is directly related to the collinear photon- and heavy boson parton densities. The derivation of the photon density from the DIS structure function F_2 has been discussed in Ref. [59]. Here we go a different path and use the measurement of the DIS cross section for validation of the obtained photon and heavy boson densities.

The single differential DIS cross section as a function of Q^2 for $e^+p \to e^+X$ with γ -exchange is given by:

$$\frac{d\sigma_{NC}}{dQ^2} = \frac{2\pi\alpha_{\rm em}^2}{Q^4} \int_{x_{\rm min}}^1 \frac{dx}{x} \left(1 + (1 - y)^2\right) \\
\times \left(e_u^2 \left[xU(x, Q^2) + x\bar{U}(x, Q^2)\right] + e_d^2 \left[xD(x, Q^2) + x\bar{D}(x, Q^2)\right]\right) \tag{16}$$

with Q^2, x, y being the DIS variables (for pure γ -exchange $xF_3 = 0$). This equation can be written in terms of the photon density f_{γ} of eq. (7):

$$\frac{d\sigma_{NC}}{dQ^2} = \frac{4\pi^2 \alpha_{\rm em}}{Q^2} \frac{dx f_{\gamma}(x_{\rm min}, Q^2)}{dQ^2}$$
(17)

The neutral current cross section coming from Z-exchange can be written, similarly, in

terms of the Z-boson density f_Z :

$$\frac{d\sigma_{NC}}{dQ^{2}} = \frac{2\pi\alpha_{\rm em}^{2}}{16\sin^{4}\theta_{\rm W}\cos^{4}\theta_{\rm W}Q^{4}} \left[\frac{Q^{2}}{(Q^{2}+M_{\rm Z}^{2})}\right]^{2} (V_{e}^{2}+A_{e}^{2}) \int \frac{dx}{x} \left(1+(1-y)^{2}\right) \\
\times \sum_{u,d} \left((V_{i}^{2}+A_{i}^{2})\left[xF_{i}(x,Q^{2})+x\bar{F}_{i}(x,Q^{2})\right]\right) \\
= \frac{\pi^{2}\alpha_{\rm em}}{Q^{2}} \frac{V_{e}^{2}+A_{e}^{2}}{\sin^{2}\theta_{\rm W}\cos^{2}\theta_{\rm W}} \frac{dxf_{\rm Z}(x_{\rm min},Q^{2})}{dQ^{2}} \tag{19}$$

Measurements of the DIS cross section [78] can therefore be used to validate the boson densities obtained in the previous section, as the fit did not constrain the boson densities.

A comparison of the measurement of the neutral current cross section $\frac{d\sigma_{NC}}{dQ^2}$ obtained in Ref. [78] with the calculation using photon and Z-boson densities is shown in Fig. 8. The DIS cross section is measured for $y_{\rm max}=0.9$, which is translated into a lower limit on $x_{\rm min}=\frac{Q^2}{y_{\rm max}s}$. For the comparison we use the measurements with zero polarization $P_e=0$. The predictions at low Q^2 , where the photon exchange dominates, are in rather good agreement with the measurements. At larger Q^2 , where also Z-exchange becomes important, the agreement becomes worse, since the interference terms included in xF_3 are not treated here. The inclusion of γ -Z interference terms in the evolution will be addressed in future work.

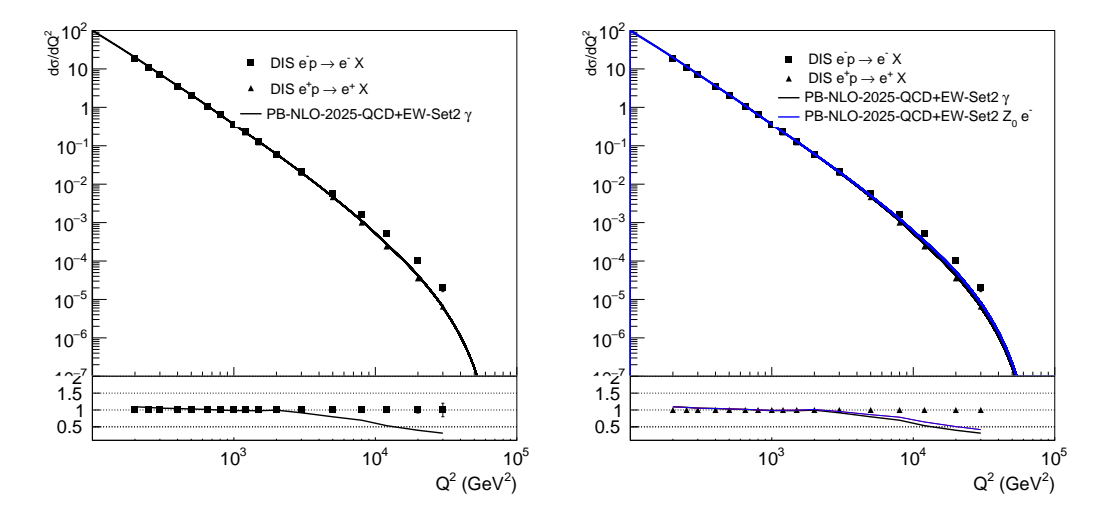


Figure 8: The measured DIS NC cross section [78] compared to the calculation using the collinear photon density (left) and the sum of $\gamma + Z$ contribution (right). The ratio shows the prediction divided by the DIS e^-p data set.

The densities for W as determined in Sec. 3.4 cannot be directly used to describe the DIS cross section, since electrons carry electroweak quantum numbers and therefore they do not represent an inclusive summation over all initial-state weak isospin charges (see discussion

in Ref. [28]), in contrast to quark states. Therefore, the different helicities must be included in the splitting functions (as detailed in eq.(2.7) of Ref. [28]). The DIS distributions $f_{\rm W}^{\rm DIS}$ are obtained using these splitting functions, instead of the unpolarized ones in eq.(10).

The charged-current DIS cross section for $e^+p \to \nu X$ with W⁺-exchange can be written in terms of the W-boson density $f_{\rm W}$ (see eq.10):

$$\frac{d\sigma_{CC}}{dQ^{2}} = \frac{G_{F}^{2}}{2\pi} \left[\frac{M_{W}^{2}}{M_{W}^{2} + Q^{2}} \right]^{2} \int \frac{dx}{x} \frac{1}{2} \left(1 + (1 - y)^{2} \right) \left[x \bar{U}(x, Q^{2}) + x D(x, Q^{2}) \right] \tag{20}$$

$$= \frac{16\pi \alpha_{\text{em}}^{2}}{128\pi \sin^{4} \theta_{\text{W}}} \frac{1}{M_{W}^{4}} \left[\frac{M_{W}^{2}}{M_{W}^{2} + Q^{2}} \right]^{2} \int \frac{dx}{x} \left(1 + (1 - y)^{2} \right) \left[x \bar{U}(x, Q^{2}) + x D(x, Q^{2}) \right] \tag{22}$$

$$= \frac{\pi^{2} \alpha_{\text{em}}}{Q^{2}} \frac{1}{\sin^{2} \theta_{\text{W}}} \frac{dx f_{\text{W+}}^{\text{DIS}}(x_{\text{min}}, Q^{2})}{dQ^{2}}$$

and similarly with W⁻-exchange (see eq.9):

$$\frac{d\sigma_{CC}}{dQ^2} = \frac{\pi^2 \alpha_{\rm em}}{Q^2} \frac{1}{\sin^2 \theta_{\rm W}} \frac{dx f_{\rm W^-}^{\rm DIS}(x_{\rm min}, Q^2)}{dQ^2}$$
(23)

In Fig. 9 the measurement of the charged current DIS cross section is compared with predictions using the W-densities. The prediction follows the general trend of the measurements, especially at small Q^2 and the suppression at large Q^2 . The predictions are within 20% for the W⁻ case.

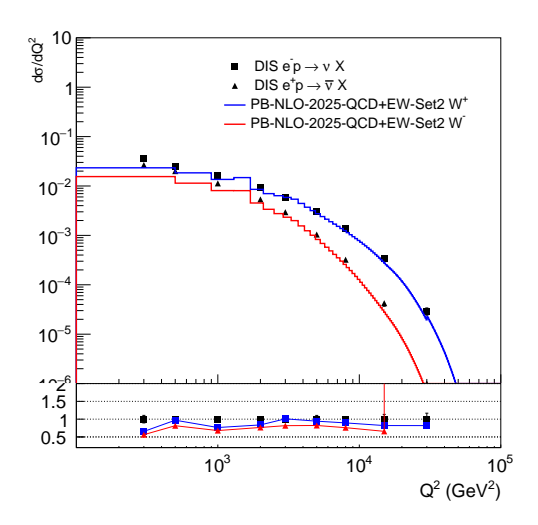


Figure 9: The measured DIS CC cross section [78] compared to the calculation using the collinear W density.

4 Conclusion

We presented a unified determination of QCD and electroweak parton densities using an extended DGLAP evolution, which is solved iteratively with the Parton Branching method allowing for a treatment of kinematic relations at each branching vertex. We apply collinear splitting functions for QCD partons at next-to-leading order accuracy, while for the photon and heavy bosons we use leading order splitting functions and couplings, in the so-called "phenomenological" scheme. Interference of γ and Z during the evolution is not considered.

The initial distributions for quarks and gluons are fitted to DIS precision data recorded at HERA. Including photon and heavy-boson contributions does not significantly alter the fit parameters or the overall fit quality. The Parton Branching method allows the simultaneous determination of transverse momentum dependent densities for the photon and heavy bosons as well.

The photon and heavy boson densities are applied to calculate the neutral and charged current cross section in deep inelastic scattering as a function of Q^2 and the comparison with measurements from HERA showed reasonable agreement. This comparison favors the treatment of the heavy boson mass as an additional propagator term, in contrast to an approach with a sharp mass cut or those which limit the z-integration by a mass dependent term.

The collinear and TMD densities for QCD partons as well as for photons and heavy electroweak bosons are, to our knowledge, the first such determinations directly fitted to DIS precision data. The densities are available in LHAPDF and TMDlib formats.

Acknowledgements. We are grateful for many discussions with A. Bagdatova, S. Baranov, A. Kotikov, A. Lipatov, M. Malyshev G. Lykasov and the other participants of the Weekly-Offline Meeting during the past years. We thank A. Glazov for constructive comments and suggestions.

Appendices

A Input parameters and input scheme

We work in the (α_0, G_μ, m_Z) scheme [79], with input parameters α_0 , G_μ and the mass of the Z-boson m_Z . The advantage of this scheme is that the independent parameters are well known experimentally with high precision. In this scheme, the weak mixing angle $\sin^2\theta_W$ as well as the mass of the W-boson m_W are derived from the input parameters, at lowest order given by:

$$(1 - \sin^2 \theta_{\rm W}) \sin^2 \theta_{\rm W} = \frac{\pi \alpha_0}{\sqrt{2G_\mu m_{\rm Z}^2}}$$

$$\cos^2 \theta_{\rm W} = 1 - \sin^2 \theta_{\rm W}, \quad \cos^2 \theta_{\rm W} = \frac{m_{\rm W}^2}{m_{\rm Z}^2}$$
(24)

$$\sin^2 \theta_{\rm W} = \frac{1}{2} - \sqrt{\frac{1}{4} - \frac{\pi \alpha_0}{\sqrt{2} G_\mu m_{\rm Z}^2}}, \quad m_{\rm W}^2 = \frac{\pi \alpha_0}{\sqrt{2} G_\mu \sin^2 \theta_{\rm W}}$$
 (25)

We list below the EW input parameters [77]:

$$G_{\mu} = 1.1663788(6) \times 10^{-5} \, \mathrm{GeV}^{-2}$$

 $\alpha_0 = 1/137.035999084(21)$
 $M_{\mathrm{Z}} = 91.1880(20) \, \mathrm{GeV}$
 $M_{\mathrm{W}} = 80.3692(133) \, \mathrm{GeV}$

B Electroweak splitting functions

In Tab. B we give an overview of the splitting functions at leading order. A full account including different polarization states is given in Refs. [29,31–33,35,70].

C Transverse Momentum Distributions

In Fig. 10 we show the transverse momentum distribution of quarks and gluons at $\mu=100$ GeV and x=0.01, including only uncertainties coming from the measurements, the model uncertainties are not shown explicitly. Especially for the bosons in Fig. 11 and 12, one can observe fluctuations in the distributions, which come from the number of simulated events $(N=10^{10})$ in UPDFEVOLV2, applying a Monte Carlos approach with forward evolution. This approach suffers from large weight fluctuations, especially for the case of heavy bosons, resulting in fluctuations in the differential $k_{\rm T}$ -distributions. The model uncertainties, as obtained from the integrated distributions (see Figs. 4 and 5) are of the same order as the statistical fluctuations obtained in the TMD distributions, and are therefore not shown.

In TMD density for photons is shown in Fig. 11, the one for heavy bosons in Fig. 12.

References

- [1] CTEQ collaboration, "CTEQ Global QCD Analyses". Webpage, 2025.
- [2] T.-J. Hou et al., "New CTEQ global analysis of quantum chromodynamics with high-precision data from the LHC", *Phys. Rev. D* **103** (2021) 014013, arXiv:1912.10053.
- [3] CTEQ-TEA Collaboration, "The photon content of the neutron", JHEP **04** (2024) 022, arXiv: 2305.10497.
- [4] MSHT collaboration, "MSHT parton densities". Webpage, 2025.

Splitting function	Diagram	V = g	$V = \gamma$	V = Z	V = W
$P_{qq}(z) = \frac{\alpha_{\text{eff}}}{2\pi} \frac{1+z^2}{1-z}$		$C_F lpha_{ m s}$	$lpha_{em}$	$\frac{\alpha_{em}(V_f^2 + A_f^2)}{4\sin^2\theta_W \cos^2\theta_W}$	$\frac{\alpha_{em} V_{qq} ^2}{4\sin^2\theta_W}$
$P_{qV}(z) = \frac{\alpha_{\text{eff}}}{2\pi} \left(z^2 + (1-z)^2 \right)$		$T_R lpha_{ m s}$	$lpha_{em}$	$\frac{\alpha_{em}(V_f^2 + A_f^2)}{4\sin^2\theta_W \cos^2\theta_W}$	$\frac{\alpha_{em} V_{qq} ^2}{4\sin^2\theta_W}$
$P_{Vq}(z) = \frac{\alpha_{\text{eff}}}{2\pi} \frac{1 + (1-z)^2}{z}$		$C_Flpha_{ m s}$	$lpha_{em}$	$\frac{\alpha_{em}(V_f^2 + A_f^2)}{4\sin^2\theta_W \cos^2\theta_W}$	$\frac{\alpha_{em} V_{qq} ^2}{4\sin^2\theta_W}$
$P_{VV'}(z) = \frac{\alpha_{\text{eff}}}{2\pi} 2\left(\frac{1-z}{z} + \frac{z}{1-z} + z(1-z)\right)$		$C_A lpha_{ m s}$	0	$4\pi lpha_{em}$ cot	$e^2 heta_W$

Table 4: Splitting functions at leading order and $\alpha_{\rm eff}$ for QCD and electroweak processes with the color factors $C_F=4/3$, $C_A=3$ and $T_R=1/2$.

- [5] L. A. Harland-Lang, A. D. Martin, R. Nathvani, and R. S. Thorne, "Ad Lucem: QED Parton Distribution Functions in the MMHT Framework", Eur. Phys. J. C 79 (2019) 811, arXiv:1907.02750.
- [6] T. Cridge, L. A. Harland-Lang, A. D. Martin, and R. S. Thorne, "QED parton distribution functions in the MSHT20 fit", Eur. Phys. J. C 82 (2022) 90, arXiv: 2111.05357.
- [7] T. Cridge, L. A. Harland-Lang, and R. S. Thorne, "Combining QED and approximate N³LO QCD corrections in a global PDF fit: MSHT20qed_an3lo PDFs", *SciPost Phys.* **17**

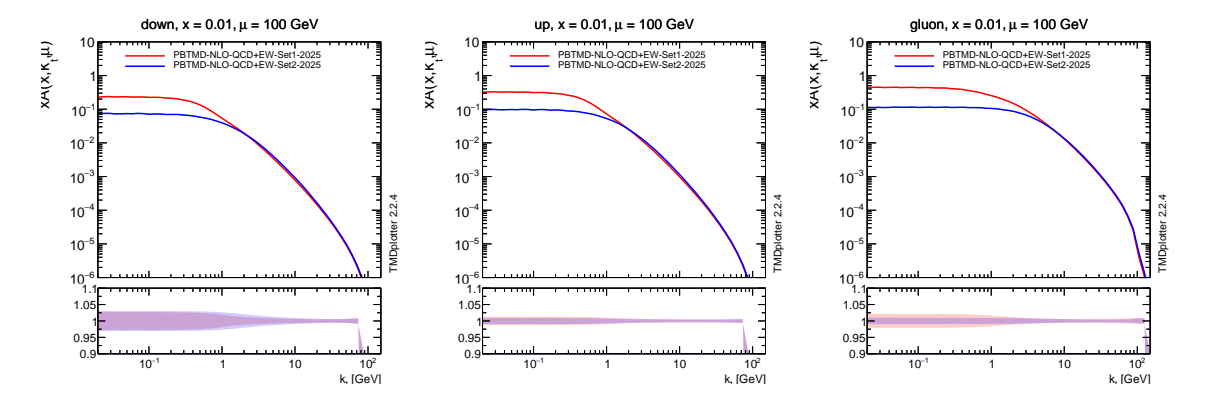


Figure 10: The transverse momentum dependent quark and gluon densities at $\mu = 100$ GeV as a function of $k_{\rm T}$. Shown are PB-NLO-QCD+EW-2025 Set1 and Set2. The uncertainty band includes only uncertainties coming from the measurements, the model uncertainties are not shown explicitly (see text).

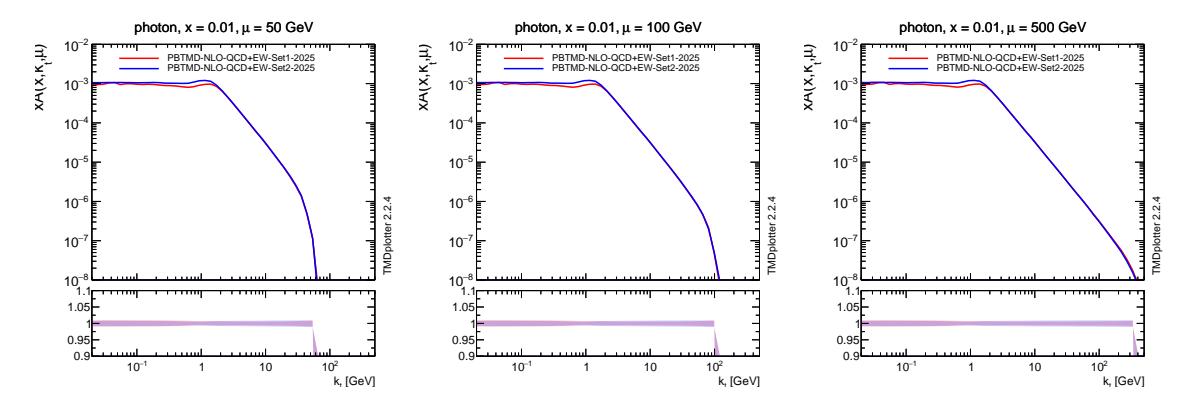


Figure 11: The TMD photon density for PB-NLO-QCD+EW-2025 Set1 and Set2 at $\mu=50$, 100 and 500 GeV as a function of $k_{\rm T}$ including uncertainties coming from the measurements, the model uncertainties are not shown explicitly (see text).

(2024) 026, arXiv: 2312.07665.

- [8] NNPDF collaboration, "NNPDF parton densities". Webpage.
- [9] NNPDF Collaboration, "The path to N³LO parton distributions", Eur. Phys. J. C **84** (2024) 659, arXiv: 2402.18635.
- [10] xFitter Developers' Team Collaboration, H. Abdolmaleki et al., "xFitter: An Open Source QCD Analysis Framework. A resource and reference document for the Snowmass study", 2022. arXiv:2206.12465.

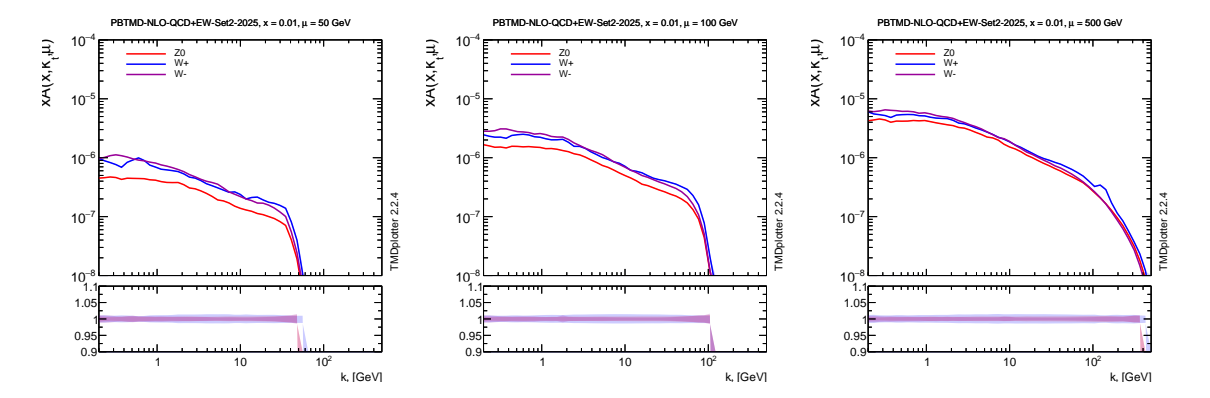


Figure 12: The TMD vector-boson density for PB-NLO-QCD+EW-2025 Set2 at $\mu=50$ GeV and $\mu=100$ GeV as a function of $k_{\rm T}$ including uncertainties coming from the measurements, the model uncertainties are not shown explicitly (see text).

- [11] S. Alekhin et al., "HERAFitter, Open Source QCD Fit Project", Eur. Phys. J. C 75 (2015) 304, arXiv:1410.4412.
- [12] A. Buckley et al., "LHAPDF6: parton density access in the LHC precision era", Eur. Phys. J. C 75 (2015) 132, arXiv:1412.7420.
- [13] S. Dawson, "The Effective W Approximation", Nucl. Phys. B 249 (1985) 42.
- [14] G. L. Kane, W. Repko, and W. Rolnick, "The Effective W+-, Z0 Approximation for High-Energy Collisions", *Phys. Lett. B* **148** (1984) 367.
- [15] Z. Kunszt and D. E. Soper, "On the Validity of the Effective W Approximation", Nucl. Phys. B 296 (1988) 253.
- [16] M. S. Chanowitz and M. K. Gaillard, "The TeV Physics of Strongly Interacting W's and Z's", Nucl. Phys. B **261** (1985) 379.
- [17] V. M. Budnev, I. F. Ginzburg, G. V. Meledin, and V. G. Serbo, "The Two photon particle production mechanism. Physical problems. Applications. Equivalent photon approximation", *Phys. Rept.* **15** (1975) 181.
- [18] S. Frixione, M. L. Mangano, P. Nason, and G. Ridolfi, "Improving the Weizsacker-Williams approximation in electron - proton collisions", *Phys. Lett.* B319 (1993) 339, arXiv:hep-ph/9310350.
- [19] C. F. von Weizsacker, "Radiation emitted in collisions of very fast electrons", *Z. Phys.* **88** (1934) 612.

- [20] E. J. Williams, "Nature of the high-energy particles of penetrating radiation and status of ionization and radiation formulae", *Phys. Rev.* **45** (1934) 729.
- [21] I. Alikhanov, "The equivalent vector boson approximation at threshold energies", arXiv:1812.05578.
- [22] J. Brehmer, J. Jaeckel, and T. Plehn, "Polarized WW Scattering on the Higgs Pole", *Phys. Rev. D* **90** (2014) 054023, arXiv:1404.5951.
- [23] K. Hagiwara, Q. Li, and K. Mawatari, "Jet angular correlation in vector-boson fusion processes at hadron colliders", *JHEP* **07** (2009) 101, arXiv:0905.4314.
- [24] D. A. Dicus, K. J. Kallianpur, and S. S. D. Willenbrock, "Higgs Boson Pair Production in the Effective W Approximation", *Phys. Lett. B* **200** (1988) 187.
- [25] G. Altarelli, B. Mele, and F. Pitolli, "Heavy Higgs Production at Future Colliders", *Nucl. Phys. B* **287** (1987) 205.
- [26] M. J. Duncan, G. L. Kane, and W. W. Repko, "W W Physics at Future Colliders", *Nucl. Phys. B* **272** (1986) 517.
- [27] S. S. D. Willenbrock and D. A. Dicus, "Production of Heavy Quarks from W Gluon Fusion", *Phys. Rev. D* **34** (1986) 155.
- [28] R. Ruiz, A. Costantini, F. Maltoni, and O. Mattelaer, "The Effective Vector Boson Approximation in high-energy muon collisions", *JHEP* **06** (2022) 114, arXiv:2111.02442.
- [29] B. Fornal, A. V. Manohar, and W. J. Waalewijn, "Electroweak Gauge Boson Parton Distribution Functions", *JHEP* **05** (2018) 106, arXiv:1803.06347.
- [30] C. W. Bauer, N. Ferland, and B. R. Webber, "Combining initial-state resummation with fixed-order calculations of electroweak corrections", *JHEP* **04** (2018) 125, arXiv:1712.07147.
- [31] C. W. Bauer, N. Ferland, and B. R. Webber, "Standard Model Parton Distributions at Very High Energies", *JHEP* **08** (2017) 036, arXiv:1703.08562.
- [32] J. Chen, T. Han, and B. Tweedie, "Electroweak Splitting Functions and High Energy Showering", JHEP 11 (2017) 093, arXiv:1611.00788.
- [33] S. Dittmaier and M. Reyer, "Electroweak splitting functions in the Standard Model and beyond", arXiv: 2507.06568.
- [34] M. Ciafaloni, P. Ciafaloni, and D. Comelli, "Towards collinear evolution equations in electroweak theory", *Phys. Rev. Lett.* **88** (2002) 102001, arXiv:hep-ph/0111109.

- [35] P. Ciafaloni and D. Comelli, "Electroweak evolution equations", *JHEP* 11 (2005) 022, arXiv:hep-ph/0505047.
- [36] A. G. Bagdatova and S. P. Baranov, "Polarization and kinematic properties of the splitting functions $q \rightarrow W \pm + q'$ and $q \rightarrow Z0 + q''$, *Mod. Phys. Lett. A* **40** (2025) 2450230, arXiv: 2404.10832.
- [37] M. Mendizabal Morentin, "Z boson production in association with jets: measurement and phenomenology". PhD thesis, Hamburg University, 2024.
- [38] ATLAS Collaboration Collaboration, "Measurements of the production cross section of a Z boson in association with high transverse momentum jets in pp collisions at $\sqrt{s}=13$ TeV with the ATLAS detector", technical report, CERN, Geneva, Jul, 2021. All figures including auxiliary figures are available at https://atlas.web.cern.ch/Atlas/GROUPS/PHYSICS/CONFNOTES/ATLAS-CONF-2021-033.
- [39] J. R. Christiansen and T. Sjöstrand, "Weak Gauge Boson Radiation in Parton Showers", *JHEP* **04** (2014) 115, arXiv:1401.5238.
- [40] F. Hautmann et al., "Collinear and TMD quark and gluon densities from Parton Branching solution of QCD evolution equations", *JHEP* **01** (2018) 070, arXiv:1708.03279.
- [41] F. Hautmann et al., "Soft-gluon resolution scale in QCD evolution equations", *Phys. Lett. B* **772** (2017) 446, arXiv:1704.01757.
- [42] H. Jung, A. Lelek, K. M. Figueroa, and S. Taheri Monfared, "The Parton Branching evolution package uPDFevolv2", arXiv:2405.20185.
- [43] V. N. Gribov and L. N. Lipatov, "Deep inelastic *ep* scattering in perturbation theory", *Sov. J. Nucl. Phys.* **15** (1972) 438. [Yad. Fiz.15,781(1972)].
- [44] L. N. Lipatov, "The parton model and perturbation theory", Sov. J. Nucl. Phys. 20 (1975) 94. [Yad. Fiz.20,181(1974)].
- [45] G. Altarelli and G. Parisi, "Asymptotic freedom in parton language", Nucl. Phys. B 126 (1977) 298.
- [46] Y. L. Dokshitzer, "Calculation of the structure functions for Deep Inelastic Scattering and e^+e^- annihilation by perturbation theory in Quantum Chromodynamics.", Sov. Phys. JETP 46 (1977) 641. [Zh. Eksp. Teor. Fiz.73,1216(1977)].
- [47] W. L. van Neerven and A. Vogt, "Improved approximations for the three loop splitting functions in QCD", *Phys. Lett. B* **490** (2000) 111, arXiv:hep-ph/0007362.

- [48] S. Moch, J. A. M. Vermaseren, and A. Vogt, "The Three loop splitting functions in QCD: The Nonsinglet case", *Nucl. Phys.* **B688** (2004) 101, arXiv:hep-ph/0403192.
- [49] A. Vogt, S. Moch, and J. A. M. Vermaseren, "The Three-loop splitting functions in QCD: The Singlet case", *Nucl. Phys.* **B691** (2004) 129, arXiv:hep-ph/0404111.
- [50] J. Vermaseren, A. Vogt, and S. Moch, "The Third-order QCD corrections to deep-inelastic scattering by photon exchange", Nucl. Phys. B724 (2005) 3, arXiv:hep-ph/0504242.
- [51] J. Blümlein, P. Marquard, C. Schneider, and K. Schönwald, "The three-loop unpolarized and polarized non-singlet anomalous dimensions from off shell operator matrix elements", *Nucl. Phys. B* **971** (2021) 115542, arXiv:2107.06267.
- [52] J. Blümlein, P. Marquard, C. Schneider, and K. Schönwald, "The massless three-loop Wilson coefficients for the deep-inelastic structure functions F_2 , F_L , xF_3 and g_1 ", JHEP 11 (2022) 156, arXiv: 2208.14325.
- [53] J. Ablinger et al., "The transition matrix element Agq(N) of the variable flavor number scheme at $\mathcal{O}(\alpha_s^3)$ ", Nucl. Phys. B 882 (2014) 263, arXiv:1402.0359.
- [54] J. Ablinger et al., "The three-loop splitting functions $P_{qg}^{(2)}$ and $P_{gg}^{(2,N_F)}$ ", Nucl. Phys. B **922** (2017) 1, arXiv:1705.01508.
- [55] S. Moch, J. A. M. Vermaseren, and A. Vogt, "The Three-Loop Splitting Functions in QCD: The Helicity-Dependent Case", Nucl. Phys. B 889 (2014) 351, arXiv:1409.5131.
- [56] A. Behring et al., "The Polarized Three-Loop Anomalous Dimensions from On-Shell Massive Operator Matrix Elements", Nucl. Phys. B 948 (2019) 114753, arXiv:1908.03779.
- [57] J. Blümlein, P. Marquard, C. Schneider, and K. Schönwald, "The three-loop polarized singlet anomalous dimensions from off-shell operator matrix elements", *JHEP* **01** (2022) 193, arXiv:2111.12401.
- [58] H. Jung, S. T. Monfared, and T. Wening, "Determination of collinear and TMD photon densities using the Parton Branching method", *Physics Letters B* 817 (2021) 136299, arXiv: 2102.01494.
- [59] A. V. Manohar, P. Nason, G. P. Salam, and G. Zanderighi, "The Photon Content of the Proton", JHEP 12 (2017) 046, arXiv:1708.01256.
- [60] C. Schmidt, J. Pumplin, D. Stump, and C. P. Yuan, "CT14QED parton distribution functions from isolated photon production in deep inelastic scattering", *Phys. Rev.* D93 (2016) 114015, arXiv:1509.02905.

- [61] A. Manohar, P. Nason, G. P. Salam, and G. Zanderighi, "How bright is the proton? A precise determination of the photon parton distribution function", *Phys. Rev. Lett.* **117** (2016) 242002, arXiv:1607.04266.
- [62] NNPDF Collaboration, "Parton distributions with QED corrections", *Nucl. Phys.* **B877** (2013) 290–320, arXiv:1308.0598.
- [63] A. D. Martin, R. G. Roberts, W. J. Stirling, and R. S. Thorne, "Parton distributions incorporating QED contributions", Eur. Phys. J. C39 (2005) 155, arXiv:hep-ph/0411040.
- [64] M. Roth and S. Weinzierl, "QED corrections to the evolution of parton distributions", *Phys.Lett.B* **590** (2004) 190, arXiv:hep-ph/0403200.
- [65] M. Gluck, C. Pisano, and E. Reya, "The Polarized and unpolarized photon content of the nucleon", *Phys. Lett. B* **540** (2002) 75–80, arXiv:hep-ph/0206126.
- [66] J. Lindfors, "Distribution Functions for Heavy Vector Bosons Inside Colliding Particle Beams", Z. Phys. C **28** (1985) 427.
- [67] R. N. Cahn, "Production of Heavy Higgs Bosons: Comparisons of Exact and Approximate Results", Nucl. Phys. B 255 (1985) 341. [Erratum: Nucl.Phys.B 262, 744 (1985)].
- [68] R. Kleiss and W. J. Stirling, "Anomalous High-energy Behavior in Boson Fusion", *Phys. Lett. B* **182** (1986) 75.
- [69] S. Dawson and S. S. D. Willenbrock, "Heavy Fermion Production in the Effective W Approximation", *Nucl. Phys. B* **284** (1987) 449.
- [70] P. Ciafaloni, G. Co', D. Colferai, and D. Comelli, "Electroweak evolution equations and isospin conservation", *JHEP* **07** (2024) 237, arXiv:2403.08583.
- [71] H1 and ZEUS Collaboration, "Combination of measurements of inclusive deep inelastic $e^{\pm}p$ scattering cross sections and QCD analysis of HERA data", Eur. Phys. J. C 75 (2015) 580, arXiv:1506.06042.
- [72] A. Bermudez Martinez et al., "Collinear and TMD parton densities from fits to precision DIS measurements in the parton branching method", *Phys. Rev. D* **99** (2019) 074008, arXiv:1804.11152.
- [73] xFitter Developers' Team Collaboration, "The photon PDF from high-mass Drell–Yan data at the LHC", Eur. Phys. J. C 77 (2017) 400, arXiv:1701.08553.
- [74] I. Bubanja et al., "The small $k_{\rm T}$ region in Drell–Yan production at next-to-leading order with the parton branching method", Eur. Phys. J. C 84 (2024) 154, arXiv:2312.08655.

- [75] I. Bubanja et al., "Center-of-mass energy dependence of intrinsic-k_T distributions obtained from Drell–Yan production", Eur. Phys. J. C **85** (2025) 278, arXiv:2404.04088.
- [76] J. Pumplin et al., "Uncertainties of predictions from parton distribution functions. 2. The Hessian method", *Phys.Rev.* **D65** (2001) 014013, arXiv:hep-ph/0101032.
- [77] Particle Data Group Collaboration, "Review of particle physics", *Phys. Rev. D* **110** (2024) 030001.
- [78] H1 Collaboration, "Inclusive Deep Inelastic Scattering at High Q^2 with Longitudinally Polarised Lepton Beams at HERA", *JHEP* **09** (2012) 061, arXiv:1206.7007.
- [79] M. Chiesa, C. L. Del Pio, and F. Piccinini, "On electroweak corrections to neutral current Drell–Yan with the POWHEG BOX", Eur. Phys. J. C 84 (2024) 539, arXiv: 2402.14659.